CONFIDENTIAL. Limited circulation. For review only
IEEE T-RO Submission no.: 17-0419.1

Stability and Robustness of Virtual Torsion Sensor for Control of Flexible Joint Robots

Michael Ruderman, *Senior Member, IEEE*

***Abstract*—The virtual torsion sensor (VTS) aims at observing the nonlinear deflection in flexible joints of serial kinematics robot manipulators and using it in the feedback position control to improve accuracy of the robot links. This model-based approach uses the motor-side sensing only, therefore replacing the load-side encoders at zero hardware costs. Since operating in the closed control loop the stability and robustness of using the VTS are crucial for its practical application. The paper extends the previous stability and robustness analysis by the case of nonlinear joint stiffness with hysteresis and provides the straightforward conditions with respect to the underlying system dynamics. The dissipativity and passivity of the torsion-torque hysteresis map is analyzed and discussed in details. The absolute stability of VTS inclusion into the position control loop is shown based on the equivalent loop transformations and Popov criteria including the sector conditions. Illustrative numerical examples of the control error dynamics and its convergence are provided.**

***Index Terms*—Flexible joint robot, hysteresis, joint torsion, robot control, virtual torsion sensor, dissipativity**

I. INTRODUCTION

Analysis, modeling, and control of robotic manipulators with flexible joints have been, and still remain, a challenging topic for both, theory and practice, see e.g. [1]–[4] and [5]–[9]. The ongoing trends towards more lightweight and flexible structures reinforce the significance of flexible joints in nowadays and future robotics. Among the related issues are the sensor reduction and, at the same time, enhanced accuracy requirements posed on positioning of the robot end-tools and, as consequence, single robot links.

An inherent problem with elasticities in robotic joints is that these are mostly nonlinear in torque-torsion characteristics, and subject to the state memory due to internal friction, structural damping, mechanical losses, and other hidden effects [10]. Note that the impact of linear joint elasticities on the robot modeling and regulation has been widely elaborated in control design [1], [2], [6], [11]–[14]. It has been shown, for positioning in [12] and later for trajectory tracking in [15], how the desired motor trajectory can be obtained from that of the joint link when accounting for linear joint elasticities. Several works [16]–[20] have been also concerned with analysis and modeling of nonlinear, correspondingly hysteretic, behavior of the joint transmissions, particularly those based on harmonic drive gearing. However up to date, the hysteresis-related problems in elastic robotic joints have not yet been efficiently solved in terms of the precise position control of the joint loads. This is especially relevant in case when the motor-side sensing (encoders) only are available for the motion control. It can be noted that up to date, very few robot manipulator solutions, like a prominent example of the lightweight manipulator [21], with an embedded link-side sensing are available. Notwithstanding, the issues related to hysteresis torsion-torque characteristics have been also acknowledged for such manipulators, see [22].

Obviously, the hysteresis-type nonlinearities in flexible joints provide remarkable challenges for dynamics analysis and control design. This is, above all, due to a cumbersome proof of the closed-loop stability and nontrivial trajectory solutions provoked by hysteresis in feedback. Little works with application examples can be found in the literature dealing with analysis of system dynamics incorporating hysteresis in feedback. When dealing with stability for nonlinear feedback systems the most developments assume a memoryless nonlinearity, see former works [23], [24] and seminal literature like e.g. [25]. Some fundamental analysis of nonlinear feedback systems having memory lead back to the works of Yakubovich e.g. [26]. In [27] an example of considering a hysteresis relay element in feedback and analyzing the associated hybrid dynamics can be found. Also in [28] the control stability of dynamic system with hysteresis in feedback has been analyzed, based on the passivity approach. However, it is not hysteresis output but its time derivative that has been considered in the feedback loop. More recent work [29] analyzes the absolute stability of linear systems with hysteresis feedback. The hysteresis nonlinearity is requested to be a Duhem hysteresis operator [30] and the shown examples are restricted to the second-order dynamics.

The aim of this paper is to analyze stability and robustness of including the virtual torsion sensor (VTS) into the control loop of flexible joint manipulators with hysteresis in torsion-torque characteristics. The VTS has been proposed and elaborated in [31]–[34], also with experimental results accomplished on a single joint setup with harmonic-drive gearing, which disclosed the nonlinear stiffness with low hysteresis distortion. Despite the VTS concept yielded a suitable approach evaluated within both numerical simulations and experiments, the stability analysis of VTS inclusion relied rather on the mild assumptions of inherently dissipative nature of hysteresis and herewith associated structural damping.

The recent work partially bases on the preliminary results of stability analysis of VTS inclusion provided in [35], where the case of nonlinear stiffness without hysteresis has been addressed. In what follows the problem of VTS inclusion into the control of flexible robot joints is formulated in Sections II

Manuscript received XXX, 2017

M. Ruderman is with Faculty of Engineering and Science, University of Agder, 4879 Grimstad, Norway. E-mail: michael.ruderman@uia.no

and III. Section IV is discussing dissipativity and passivity of the torsion-torque hysteresis map with a detailed analysis of two boundary cases of zero and maximal energy dissipations on the input cycles. The absolute stability of VTS inclusion into the control loop is shown in Section V. Illustrative numerical examples are also given. Concluding remarks are drawn in Section VI.

II. CONTROL OF FLEXIBLE ROBOT JOINTS

Considering the vectors of motor coordinates $\theta \in \mathbb{R}^n$, link coordinates $q \in \mathbb{R}^n$, and relative displacement between both $x = \theta - q$, the dynamics of a flexible joints robotic manipulator can be written as

$$H\ddot{q} + \Phi(q,t) = h(x) + D\dot{x}, \quad (1)$$
$$J\ddot{\theta} + h(x) + D\dot{x} = u(t) - f(t). \quad (2)$$

Here the lumped link and motor inertias are denoted by H and J correspondingly. Note that the link inertias H are assumed as already decoupled from the configuration-dependent inertia terms. The residual configuration-dependent inertia terms, together with another coupling effects of the manipulator dynamics, including Coriolis-centrifugal and gravity, are summarized in a generalized nonlinear function $\Phi(\cdot)$. It is assumed that Φ can be decoupled, or at least minimized, by an inverse model-based torque control acting either in feedback, i.e. feedback linearization, or feed-forward, see e.g. [36], [37] for details. The transmitted torque, respectively reactive joint torque, is

$$\tau = h(x) + D\dot{x}, \quad (3)$$

where the rate-independent nonlinear stiffness map is h and the viscous damping coefficient is D. The overall joint motor friction

$$f = B\dot{\theta} + \beta(\dot{\theta})$$

is assumed to be a linear combination of the viscous term, which is the linear motor damping, and nonlinear friction term β. The latter is understood to be dissipative, see e.g. [38], [39] for details, and amplitude-bounded like e.g. Coulomb friction at unidirectional motion. Note that f is assumed to be known at the stage of designing and applying the VTS. During analysis of VTS inclusion, provided in Section V, the friction f can be deliberately neglected for the sake of simplicity, since it acts as an additional motor-side damping. Therefore assuming $f = 0$ is dealing with rather under-damped 'worst case' when analyzing the closed loop system stability.

For possibly fast dynamic response of the controlled robotic manipulator a model-based torque feed-forward control is a common praxis, see e.g. [36], [37] for details. That means given the reference joint trajectory $\theta_r(t) \in \mathcal{C}^2$, the centralized manipulator dynamics model computes the required motor torques u_{ff} which are directly applied to drive the system (1), (2). Note that the reference trajectory should be at least twice continuously differentiable so as to allow for solving the inverse dynamics which includes the acceleration-dependent terms. In order to avoid jerks and to reduce excitation of the transient joint oscillations the reference trajectory can be required to have higher order of continuity, like e.g. $\mathcal{C}^3$ or $\mathcal{C}^4$. It is also worth noting that the model-based torque feed-forwarding mostly relies on the assumed rigid manipulator dynamics so that no explicit joint flexibilities, as in (1), (2), are taken into consideration when computing $u_{ff}\big(\theta_r(t)\big)$. This is mostly due to complexity of the resulted inverse dynamics model with high-order derivatives of the states and state-dependent matrices, which should be solved in real-time. However, the full-order inverse dynamics feed-forward control for flexible joint robots can be found, for linear joint stiffness in [40] and for nonlinear joint stiffness with hysteresis in [34].

Assuming the inherent modeling errors and system uncertainties in (1), (2) the residual control error $e = \theta_r - \theta$ can be traditionally compensated by the proportional derivative (PD) feedback control so that the total control vector results in

$$u = u_{ff} + K_p\, e + K_d\, \dot{e}. \quad (4)$$

Note that the feedback control gains $K_p, K_d > 0$ allow for a robust and design-specific shaping of the error dynamics, and that in terms of the bandwidth and damping as well.

The residual error dynamics of system (1), (2) with the control law (4) can be written as

$$\tilde{H}(q)\ddot{q} - h(x) - D\dot{x} = 0, \quad (5)$$
$$J\ddot{e} + (D + K_d)\dot{e} + K_p\, e + h(x) - D\dot{q} = 0. \quad (6)$$

Note that the eliminated feed-forward control part is to compensate for both the motor friction and configuration-dependent manipulator dynamics as well. While the first implies directly since the friction disturbance is matched with the control input, the second is possible under the milde assumptions $\theta \approx q$, $\dot{\theta} \approx \dot{q}$. That holds once the relative displacement x is bounded and relatively low, comparing to the motor and link displacements, and $\dot{x}$ is sufficiently damped by the joint structure. Further we note that (5) still confronts with the whole configuration-dependent inertia matrix $\tilde{H}$, since the residual control errors excite the manipulator dynamics that cannot be compensated by feed-forwarding. Since the configuration-dependent inertia matrix of manipulator is upper and lower bounded, see e.g. [36], [37] for details, one can write $H_{\min} \leq \tilde{H}(q) \leq H_{\max}$, which is sufficient for analysis. Note that here and further on the dynamics (5), (6) will be interpreted as a single-input-single-output (SISO) system by considering any single decoupled robotic joint, with the upper and lower boundaries of the link inertia as above.

III. VIRTUAL TORSION SENSOR

The VTS, introduced and elaborated in control in [31], [33], [34], aims at predicting the relative joint torsion by means of the observed reactive joint torque which is, subsequently, mapped through the inverse torsion-torque function. The latter can be assumed as either linear or nonlinear and incorporates hysteresis memory as well – the general case we will assume in the following. Independently on the underlying model, the inverse hysteresis map should be deterministic for the given initial state and input series and computable in real-time. The observation of reactive joint torque bases on an approach known as generalized momenta, for details we refer

CONFIDENTIAL. Limited circulation. For review only
IEEE T-RO Submission no.: 17-0419.1

to [41], [42]. In the following, the concept of VTS is briefly summarized while for more details we refer to [31], [33], [34].

Assuming the generalized momenta as $p = J\dot{\theta}$, the dynamics of the joint actuator (2) can be rewritten as

$$\dot{p} = u - f(\dot{\theta}) - \tau. \tag{7}$$

Here we note that the drive torque u and friction torque f are known for the available measurements. The former in directly deduced from the motor current for the known motor torque constant. The latter is provided by the identified friction model for which the measured motor velocity serves as an input. The dynamic behavior of the generalized momenta can be estimated by

$$\dot{\tilde{p}} = u - f(\dot{\theta}) - r, \tag{8}$$

where the residual state $r = L(\tilde{p} - p)$ is proportional to the estimation error. The constant $L > 0$ is the design parameter of VTS to be assigned. It can be shown that since

$$r = L\Big(\int \big[u - f(\dot{\theta}) - r\big]\mathrm{d}t - p\Big), \tag{9}$$

the residual state dynamics offers an always stable first-order behavior described by

$$\dot{r} + Lr = L\tau. \tag{10}$$

It is evident that the residual state r follows the unknown joint torque τ while being lagged behind it by the time constant L^{-1}. Both values at steady-state coincide with each other. Note that the observation gain L constitutes a trade-off between the fast observer convergence and amplification of the measurement noise. The measurement noise is partially reduced due to the integrator averaging, cf. (9), though cannot be fully neglected due to the simultaneous impact of the measured u and $\dot{\theta}$ quantities.

The reactive joint torque, observed as described above, serves as an input of the inverse torsion-torque map. Assuming a nonlinear and rate-independent map $\tau = h(x)$ is given, the VTS-predicted joint torsion results in

$$\tilde{x} \approx h^{-1}(r). \tag{11}$$

Here we note that an exact equality in (11) can be guarantied for steady-state only, since the torque estimate r contains also the linear damping term proportional to $\dot{x}$, cf. with (2). However, an appropriate L assignment provides the low-pass filtering of the damping-related torque estimate, so that the estimation error $\big(h(x) - r\big) \to -\infty$ dB at low frequencies and $\big(h(x) - r\big) \to 0$ dB at higher frequencies. Note that, at the same time, the amplitude of $h(x)$-mapping is constant for all frequencies and relatively high due to a high joint stiffness.

The problem of VTS inclusion into the feedback control loop is illustrated by Fig. 1. Two concentrated inertias represent the motor and link side connected by (nonlinear) spring which imitates the flexible joint, cf. with (1), (2). Note that the configuration-dependent link inertia is assumed as decoupled, e.g. by feed-forward torque control, see Section II. The differential angular displacement x between the motor and link axes, which we will denote as *joint torsion*, deteriorates the motion control of the link. Due to a finite stiffness it produces

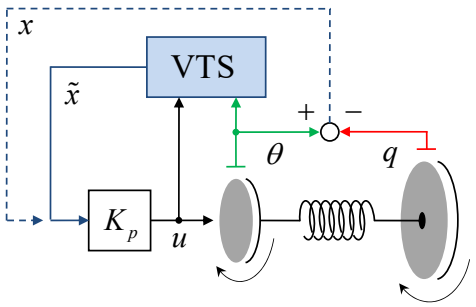

Fig. 1. Flexible robotic joint with direct and VTS-based torsion feedback.

the disturbing vibrations at the resonance frequency during the transient phases. Moreover, it distorts the steady-state accuracy of the link position at non-zero equilibrium torque, for instance due to the gravity or external forces acting on the manipulator. Recall that since the robotic manipulator is expected to drive, correspondingly position, a payload mounted on the end-effector, the control accuracy in the link space $\{q\}$ is of a primary interest. It is apparent that attenuation of the transient and steady-state link errors require, to some extent, an information on the link position, correspondingly torsion. Here we should note that the most nowadays industrial robotic manipulators are still equipped with the motor-side encoders only. An additional link state measurement can arouse an extra system redesign and hardware costs and, in several regards, can be cumbersome or even unfeasible for implementation. Obviously, an available torsion quantity can be incorporated into the motor control feedback loop, therefore providing an "offset" to the motor feedback position and therefore achieving better position accuracy in the $\{q\}$-space. Moreover, including the differential velocity $\dot{x}$ into the feedback loop can significantly reduce the disturbing link oscillations as has been shown e.g. in [2].

The VTS predicts the relative joint torsion $\tilde{x}$ by using the motor torque u and velocity $\dot{\theta}$, both available in the system. Since the relative joint torsion is used to augment the feedback motor position under control, and therefore to account for deviations between the joint input and output displacements, the proportional gain K_p of the motor controller has to be taken into consideration. The feedback motor control is assumed as available and robust, in terms of the amplitude and phase margins and external disturbance attenuation. Now the question which arises is how stable the feedback of the relative joint torsion is. Note that this can be investigated independently from the designed motor control, since the same proportional gain K_p only is used for the torsion feedback. In this case the feedback control (3), without feed-forward part, transforms to

$$u^* = K_p e + K_d \dot{e} + K_p \tilde{x}. \tag{12}$$

Therefore, the torsion feedback appears as an inner control loop nested inside of the total cascaded structure, cf. Fig. 1. Apart from the question of torsion feedback stability, inclusion of VTS instead of the real measurement requires a more detailed analysis. Note the absolute stability of VTS-

inclusion for nonlinear memoryless, i.e. without hysteresis, joint stiffness has been preliminary shown in [35].

IV. DISSIPATIVE HYSTERESIS TORQUE MAP

A. Energy dissipation and lost motion

We consider first a generalized torsion-torque hysteresis map $\tau = h(x)$ with two necessary requirements posed on that, to be rate-independent and clock-wise in the I/O (input-output) sense. The first one means that the output trajectories and therefore energy conservation, respectively dissipation, per cycle do not depend on the input velocity. Therefore, the $h(\cdot)$-map is invariant to affine transformations of time, i.e. $a + bt$ $\forall\ a \in \mathbb{R}, b \in \mathbb{R}^+$. The second requirement implies that for any pair of two output trajectory segments connected by an input reversal point it is valid that the forward segment, for which $\dot{x} > 0$, always lies above the backward segment, for which $\dot{x} < 0$. This type of nonlinear spring behavior can be directly incorporated into the stiffness term. In the structural mechanics literature it is often called as hysteresis damping or structural damping.

Since the torsion-torque map characterizes a spring element, the corresponding energy storage can be considered for any two points $x_2 > x_1$. Without loss of generality assume a pair of the input states (x_1, x_2) as depicted in Fig. 2, while x_1 represents an arbitrary initial state and x_2 represents the next reversal state of an input sequence. It is obvious that the total energy of the spring can be written as

$$E(t) = \int\limits_{X(t)} h(\sigma)\mathrm{d}\sigma + E(0), \tag{13}$$

where $X(t)$ is entire input trajectory with $X(0) = x_0$. For simplicity we will assume $E(0) = 0$. It is worth to emphasize that here no kinetic energy is to be taken into account since the torsion-torque map is rate-independent and the overall torque (or generalized force) evolution does not depend on $|\dot{x}|$.

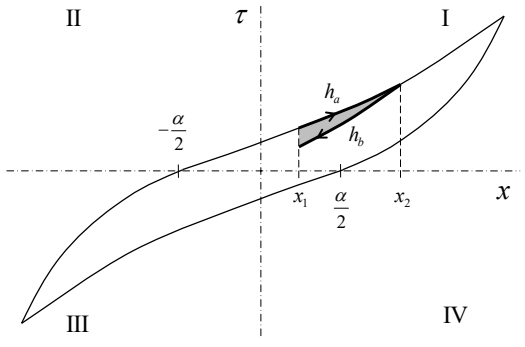

Fig. 2. Torsion-torque h-hysteresis loop with input reversal.

Coming back to the $[x_1, x_2]$ interval, it can be shown that the change in energy level between both limits is given by

$$E(x_2) - E(x_1) = \int\limits_{x_1}^{x_2} h(x)\mathrm{d}x. \tag{14}$$

If the nonlinear torsion-torque map is first assumed as none-hysteretic, then the forward and backward segments of the output trajectory coincide with each other so that

$$\Delta E_{2-1} = \int\limits_{x_1}^{x_2} h_a(x)\mathrm{d}x = -\int\limits_{x_2}^{x_1} h_a(x)\mathrm{d}x, \tag{15}$$

$$\Delta E_{1-2} = \int\limits_{x_2}^{x_1} h_a(x)\mathrm{d}x = -\int\limits_{x_1}^{x_2} h_a(x)\mathrm{d}x. \tag{16}$$

Obviously, the total energy change during one x_1-x_2-x_1 cycle is $\Delta E_{2-1} + \Delta E_{1-2} = 0$ so that the nonlinear spring behaves as lossless. That is the total potential energy stored in the rotary spring during the relative torsion can be recuperated after the twisting back. Apparently there is no damping captured by the $h(\cdot)$ function without hysteresis.

Now consider the actual hysteresis branching after the input reversal. Following the same line of arguments as above one can show that the total energy change during the same closed cycle results in

$$\Delta E_{2-1} + \Delta E_{1-2} = \int\limits_{x_1}^{x_2} h_a(x)\mathrm{d}x - \int\limits_{x_1}^{x_2} h_b(x)\mathrm{d}x = \Delta E \neq 0. \tag{17}$$

Since the first summand in (17) constitutes the potential energy which has been stored when moving from x_1 to x_2 and the second summand corresponds to the potential energy which has been released on the way back, their positive difference $\Delta E > 0$ represents the total energy losses during one x_1-x_2-x_1 cycle. Obviously it corresponds to the area of hysteresis loop, shown as grey-shaded in Fig. 2. Note that the loop should not be necessarily closed, and the corresponding area reflects the instantaneous energy losses after an arbitrary input reversal. Wider hysteresis loops generally represent larger hysteresis damping, while the closed-loop area and shape of hysteresis branches can vary depending on the input amplitude and history. Both determine the operation point within the enclosing major hysteresis loop which is characteristic for the given input range.

The temporal change of energy can be analyzed by taking the time derivative of (13) which results in

$$\dot{E}(t) = \frac{\mathrm{d}}{\mathrm{d}t}\int h(x)\mathrm{d}x = h(x)\dot{x}. \tag{18}$$

Obviously the energy change rate is proportional to that of the input, i.e. $\dot{x}$, since the latter drives the output state according to $h(x)$. Since $h(\cdot)$ is rate-independent, in other words static but at the same time multi-valued mapping, it is of interest to make a qualitative comparison of the energy changes depending on the sign of both, hysteresis output and rate of the input. Here some $|\dot{x}| = \mathrm{const}$ can be assumed. From (18) it becomes apparent that $\dot{E} > 0\ \forall\ \dot{x} > 0$ in the I quadrant and $\dot{E} > 0\ \forall\ \dot{x} < 0$ in the III quadrant of the I/O plane, cf. Fig. 2. It means that independently of hysteresis damping, the nonlinear spring behaves as a conventional one in the I and III quadrants, i.e. with increasing the potential energy during elongation for $x > 0$ and during compression for $x < 0$. Note that at $x = 0$ the spring is neither elongated nor compressed

while $h(0) \neq 0$ represent the residual stress manifesting the hysteresis. On the contrary, the II and IV quadrants can be seen as a 'reversal' spring since here the input displacement and output force have the opposite signs. However, the sign of energy changes holds according to (18). That means the I and II quadrants form a half-plane where $\dot{x} > 0$ implies $\dot{E} > 0$. Correspondingly the III and IV quadrants form the complement half-plane where $\dot{x} < 0$ implies $\dot{E} > 0$. Note that the above distinguishing between the I-IV quadrants of the I/O map does not violate the energy dissipation and therefore hysteresis damping at any reversal cycle. At the same time, it creates the effect of quasi-plasticity and residual torques at zero torsional displacement. This appearance is well-known in structural mechanics as the Bauschinger effect and described by the so-called kinematic/isotropic hardening, see e.g. [43] for details. The kinematic/isotropic hardening occurs during the cyclic loading, correspondingly deformation, and manifests in the hysteresis stress-strain curves for a given structure. Note that for moderate strains and cyclic loading applications the cyclic hardening-softening [43] provides the loop stabilization. Therefore the plastic fraction of the total strain can be assumed as relatively low, and with a constant boundary for the bounded stress range. In terms of the torsion-torque hysteresis, a constant

$$\max h^{-1}(0) - \min h^{-1}(0) := \alpha \tag{19}$$

can be therefore assigned, which we will denote as a *band* of hysteresis lost motion. Note that for symmetric hysteresis springs this band is symmetric to origin so that the quasi-plastic (residual) deformation is bounded by $[-\alpha/2, \alpha/2]$. Here we deliberately use the term quasi-plastic, since a complex mechanical assembly of flexible joint is only approximated by the nonlinear hysteresis spring, and does not constitute a single solid structure. Rather it contains a number of solid elements in contact, each one with specific geometry and stiffness, so that the clearances between them and internal frictional interactions contribute to the plastic appearance, that from an I/O point of view.

It is worth to emphasize that the hysteresis lost motion can be maximal at zero torque and is continuously decreasing with an increasing torque amplitude. Recall that the hysteresis lost motion reflects the difference between the underlying static (nonlinear) stiffness curve and the corresponding hysteresis branches for the same level of instantaneous torque, see [44] for details. The hysteresis lost motion can lead to the limited, but still inherently pronounced, link positioning errors when no load position information is used for the control. Experimental evidence of hysteresis lost motion and corresponding link positioning errors can be found in [32], [44].

B. Hysteresis spring as dissipative operator

In the previous section it has been shown that the hysteresis map $\tau = h(x)$ is dissipating energy at each input reversal. In order to be able to analyze the hysteresis as an I/O operator incorporated into dynamic loops we make use of concept of the system dissipativity, correspondingly passivity, which revealed as particularly suitable for nonlinear system analysis and control, see e.g. in literature [25], [45], after being introduced in [46]. For a static I/O map, with the input u and output y representing an "energy pair" of the physical system, a direct sector test, see [25] for details, provides a sufficient proof whether the system is passive. If for any u-value $yu \geq 0$ then the energy consumption is positive and the system is passive [47]. In other words, the I/O graph should lie within the I and III quadrants only. Since the static hysteresis map is not memoryless, cf. with [25], but represents a multi-valued function lying in all four quadrants and being always continuously increasing, the direct sector test does not provide correct conclusions about passivity. Therefore we are to take special measures, like in case of passivity analysis performed for dynamic nonlinear systems. Following to [24], a system with the state $z \in Z$ is passive if it is dissipative with the supply rate $w = \langle u, y \rangle$ and nonnegative storage function $V : Z \to \mathbb{R}$ with $V(0) = 0$, so that

$$V(z) - V(z_0) \leq \int_0^t yu \, \mathrm{d}t. \tag{20}$$

Note that $V(z)$ is a Lyapunov function candidate representing energy level of the system as function of the state. Assuming the storage function is continuously differentiable with respect to the time results in the condition for system to be passive if

$$\dot{V}(z) \leq yu, \tag{21}$$

and that independently of the initial state z_0. Obviously, the system is lossless if $\dot{V} = yu$.

Considering the hysteresis map introduced in Section IV-A, with a state given by the hysteresis output, i.e. $y = \tau$, we assume the storage function

$$V = \gamma \frac{1}{2} \tau^2 - \int_\Gamma h(x) \mathrm{d}x. \tag{22}$$

Note that Γ is the path traversed in the (x, τ) plane. The path integral captures the amount of dissipated energy once the input reverses. Regardless whether operating in the upper or lower half plane, i.e. for $\tau > 0$ or $\tau < 0$ correspondingly, one can show that for a certain $\gamma > 0$ the first summand in (22) is always larger than the second one, so that V remains nonnegative for all (x, τ) trajectories. Note that (22) belongs to a certain class of Lyapunov functionals, introduces by Yakubovich in [26] for analyzing the systems with feedback hysteresis. We also note that the first summand in (22) constitutes the potential energy of the spring, and in case of a linear stiffness it is valid $\gamma = k^{-1}$, for a positive spring constant k.

For the given I/O system we assume the supply rate

$$w(u, y) = \tau x, \tag{23}$$

and substituting it, together with the time derivative of (22), into (21) obtains

$$\gamma \, \tau \dot{\tau} - \tau \dot{x} \leq \tau x. \tag{24}$$

Further substituting τ and $\dot{\tau}$ by the hysteresis map, correspondingly its time derivative, results in

$$h(x) \Big(\gamma \frac{\partial h}{\partial x} - 1 \Big) \dot{x} \leq h(x) x. \tag{25}$$

It appears that the proof of (25) requires a case difference for all four quadrants, also for both positive and negative input velocities each. This can render our later analysis as cumbersome and unpractical in terms of incorporating hysteresis into dynamic system and control loops. Instead, we will consider two boundary cases for hysteresis $h(\cdot)$, satisfying dissipation property shown in Section IV-A, and assume that all other shapes of clockwise hysteresis are within these boundary conditions.

Consider first the upper boundary case of maximal energy dissipation at each input reversal. Assume the corresponding hysteresis map

$$\tau = \bar{h}(x) = kx + c\,\mathrm{sign}(\dot{x}). \tag{26}$$

Note that (26) remains rate-independent since the sign of the input velocity solely captures the direction changes without any input or output dynamics. One can recognize that (26) represents the case of combining the linear spring with a Coulomb-type friction, so that the amount of energy dissipated between two consecutive points $x_2 > x_1$ is

$$E_h = \int_{x_1}^{x_2} c\,\mathrm{sign}(\dot{x})\mathrm{d}x = c\,\mathrm{sign}(\dot{x})(x_2 - x_1). \tag{27}$$

Therefore, the damping rate is velocity-independent and moreover constant for any path Γ traversed in the (x, τ) plane, cf. with (22). The torsion-torque hysteresis loop parameterized by $c, k > 0$ is shown in Fig. 3 with exemplary reversal points. Note that the hysteresis loop is clockwise, and the stepwise

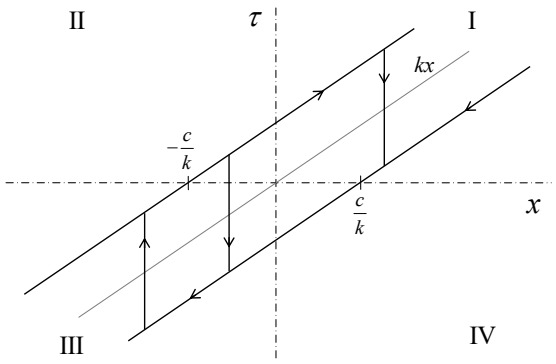

Fig. 3. Torsion-torque $\bar{h}$-hysteresis loop with input reversals.

transitions between the upper and lower slopes, $kx + c$ and $kx - c$ correspondingly, provide the maximal possible energy dissipation for each reversal cycle. The time derivative of the storage function (22) results in

$$\dot{V} = kx\dot{x} - \tau\dot{x} = -c|\dot{x}|, \tag{28}$$

from which one can see that only at zero velocity the system behaves as lossless. Otherwise, any input changes provoke the energy dissipation proportional to the magnitude of input velocity. Obviously the system is dissipative, while its passivity we should first investigate based on (23), (24). Substituting (28) and (26) into (24) results in

$$-c\,|\dot{x}| \le x\big(kx + c\,\mathrm{sign}(\dot{x})\big). \tag{29}$$

From the case difference, and that for the positive and negative input values, one can show that in order to ensure that (29) holds two conditions should be fulfilled

$$x \;\ge\; \frac{c}{k} \quad \text{if } \; x > 0 \wedge \dot{x} < 0, \tag{30}$$

$$x \;\le\; -\frac{c}{k} \quad \text{if } \; x < 0 \wedge \dot{x} > 0. \tag{31}$$

From (30), (31) one can conclude that the hysteresis map (26) is almost always passive, except a decreasing trajectory within the IV quadrant and increasing trajectory within the II quadrant. Note that if in one of both cases the input direction changes, the output immediately jumps into the sector of system passivity, i.e. I or III quadrant correspondingly. Note that the threshold values in (30), (31) correspond to the band of hysteresis lost motion, cf. with (19), so that $c/k = 1/2\alpha$. However, unlike in case of a piecewise continuous hysteresis map $h(\cdot)$, the input range $[-c/k, c/k]$ cannot be directly interpreted as a quasi-plastic residual deformation, since the output torque always belong to one of the three manifolds $\{kx-c,\, kx,\, kx+c\}$, and the discrete transitions between them only are possible. Nevertheless, the band of hysteresis lost motion keeps the same meaning since the motion would stop within it, since the spring restoring torque becomes insufficient to overcome the Coulomb friction. As implication the system becomes sticking within this band.

The lower boundary case assumes no energy dissipation at input reversals so that the same line of arguments as above can be pursed while assuming $c = 0$. This case the hysteresis in Fig. 3 'collapses' to a linear stiffness slope $\tau = kx$, thus representing a classical spring without energy losses. Substituting $c = 0$ into (29) results in

$$0 \le kx^2,$$

so that the system is always passive, and lossless as well, since $\dot{V} = \tau x$. Here we remind that if the torsion-torque map is an arbitrary static memoryless function, i.e. without hysteresis, its passivity can be directly proved by the sector condition $\underline{h}(x)x \ge 0$, cf. with [25]. Therefore no explicit analysis as above is required for this case. The absolute stability of torsion feedback for a nonlinear memoryless stiffness of the cubic polynomial form has been demonstrated for both, direct measurement and VTS-prediction, in [35]. There the well-celebrated Popov criterion, see e.g. [48] for details, has been applied. In next Section we are briefly to summarize the results from [35] a for memoryless nonlinear stiffness, before considering the hysteresis map h.

V. STABILITY OF VTS INCLUSION

A. Nonlinear memoryless stiffness

In order to analyze VTS inclusion into the closed loop, the control (12) should be extended according to Fig. 1 so that $K_p\tilde{x}$ appears on the right-hand side of error dynamics (6). Since the torsion-torque map, equally as its inverse, are static and the joint torque estimation is driven by (10) it can be assumed that the dynamic relationship between the joint torsion and its estimate is given by

$$\dot{\tilde{x}}L^{-1} + \tilde{x} = x. \tag{32}$$

Note that while certain steady-state errors between x and $\tilde{x}$ are possible, caused by the mapping errors of $h(\cdot)$, the first-order time delay behavior (32) remains always valid due to observer (7)-(10) dynamics governed by the design parameter L. The control error dynamics (5), (6), modified by VTS inclusion as above, discloses one static nonlinearity in feedback so that the overall system can be rewritten in a state-space form as

$$\dot{\mathbf{x}} = \mathbf{A}\mathbf{x} - \mathbf{b}\gamma(y), \quad y = \mathbf{c}^T\mathbf{x}. \tag{33}$$

This one is suitable for absolute stability analysis by means of the Popov or, more general, circle criteria; for details on both we refer to e.g. [48]. Decomposing the overall torsion-torque map in such a way that the linear stiffness component is in superposition with the nonlinear one

$$h(y) = ky + \gamma(y), \tag{34}$$

allows to obtain the linear matrix form

$$\mathbf{A} = \begin{bmatrix} 0 & 1 & 0 & 0 & 0 \\ -\frac{k}{H} & -\frac{D}{H} & \frac{k}{H} & \frac{D}{H} & 0 \\ 0 & 0 & 0 & 1 & 0 \\ \frac{k}{J} & \frac{D}{J} & -\frac{k+K_p}{J} & -\frac{D+K_d}{J} & \frac{K_p}{J} \\ -L & 0 & L & 0 & -L \end{bmatrix}, \tag{35}$$

$$\mathbf{b} = \left[0,\, -\frac{1}{H},\, 0,\, \frac{1}{J},\, 0\right]^T, \text{ and } \quad \mathbf{c}^T = [-1,\, 0,\, 1,\, 0,\, 0]\,. \tag{36}$$

The corresponding state vector is $\mathbf{x} = [q, \dot{q}, \theta, \dot{\theta}, \tilde{x}]$. Note that while the residual control error has been considered in (6), the above state-space model is equivalent to that when assuming zero reference value and $e(0) \neq 0$. One can easily show that the system matrix $\mathbf{A}$ is Hurwitz and the pair $[\mathbf{A}, \mathbf{b}]$ is controllable. Consequently, the first condition of the Popov's criterion is fulfilled.

The second condition concerns the static nonlinearity in feedback which has to comply with sector criterion

$$\forall y \neq 0 \;\Rightarrow\; k_1 \leq \frac{\gamma(y)}{y} \leq k_2 \tag{37}$$

for two non-negative numbers k_1 and k_2. Recall that the passivity sector condition, cf. Section IV-B, allows to restrict the above sector to $[0, k_2]$ so that the Popov's criterion is applicable instead of a more general circle criterion. The latter allows also for $k_1 < 0$. Note that in [35] it has been shown that for a bounded joint torsion, which is a reasonable assumption for real mechanical structures, the cubic polynomial nonlinearity belongs locally to the sector $[0, k_2]$ for some $x_{\min} \leq x \leq x_{\max}$, and the Popov's criterion is directly applicable. Other static nonlinear maps $\gamma(y)$ satisfying (37) for $[0, k_2]$ are equally thinkable.

The third condition of the Popov's criterion of absolute stability requires that for the transfer function

$$G(s) = \mathbf{c}^T(s\mathbf{I} - \mathbf{A})^{-1}\mathbf{b}$$

there exist a strictly positive number σ such that

$$\forall \omega \geq 0 \quad \mathrm{Re}\big[(1 + j\sigma\omega)G(j\omega)\big] + \frac{1}{k_2} \geq \varepsilon, \tag{38}$$

for any arbitrary $\varepsilon > 0$. The third condition is generally facilitated for interpretation by using the so-called Popov plot. That one visualizes the polar plot $\omega\,\mathrm{Im}\{G(j\omega)\}$ over $\mathrm{Re}\{G(j\omega)\}$ for the frequencies starting from DC, i.e. $\omega \to 0$, and going towards $\omega \to \infty$. Afterwards one can prove whether it exists a strictly positive σ for a sufficiently large k_2, so that the $1/\sigma$ slope, which goes through $-1/k_2$, does not intersect the polar plot. The Popov plots are exemplary shown in Fig. 4 for a numerical example specified further in Section V-C, once for the upper and once for the lower bound of $\tilde{H}$.

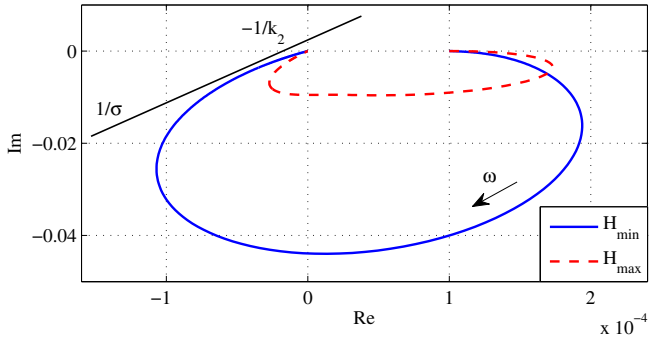

Fig. 4. Popov plots of the system (33)-(36) for $H_{\min}$ and $H_{\max}$.

B. Nonlinear stiffness with hysteresis

In order to prove the stability of system (33) in case the feedback nonlinearity contains hysteresis one can make use of the passivity theorem which says the feedback connection of two passive system is passive. That implies stability of the closed loop, or asymptotic stability in case the feedback connected systems are strictly passive. This general approach, however, challenges one to show the passivity of dynamic linear subsystem from (33) which, in turn, requires to evaluate the positive realness of the transfer function $G(s)$. The latter can be achieved by use of the well-celebrated positive real lemma, known as Kalman-Yakubovich-Popov lemma, see e.g. [25] for details. To prove the required existence of matrices satisfying the lemma's equalities can yield a challenging issue, in view of the 5×5 system matrix (35). Therefore, we pursue an alternative strategy, which again relies on the Popov's absolute stability criterion with the corresponding sector condition. The elegance of the proposed method flourishes after the corresponding nonlinearity decomposition and some minimal necessary loop transformations.

Assume that now the feedback nonlinearity has the form

$$h(y) = ky + \gamma(y) + \delta(\dot{y}), \quad \text{with} \quad \delta = c\,\mathrm{sign}(\dot{y}), \tag{39}$$

cf. with (26) and (34). Obviously, incorporation of the velocity sign extends the case we analyzed in Section V.A to the upper boundary case of hysteresis provided in Section IV.B. Since the linear stiffness k is already accumulated in the system matrix (35), and both nonlinear terms in (37) are in the algebraic superposition, two separated nonlinearity feedback loops can be considered. For the first one, the linear dynamics is $G(s)$, while for the second one it is $G(s)s$. Therefore, the system (33), (39) can be transformed into one depicted in Fig. 5. It

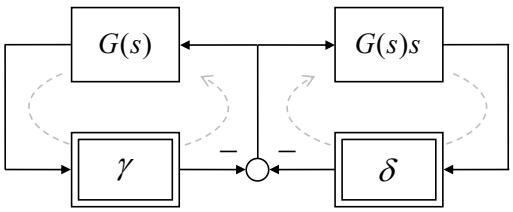

Fig. 5. Transformed loop with two feedback nonlinearities.

is apparent that the output of each nonlinearity acts on the opposite loop as an exogenous input, thus without influencing its eigen-behavior. While the absolute stability of the $G(s)\,\gamma$ loop has been proved in Section V-A, the same procedure can be applied to the $G(s)s\,\delta$ loop as follows.

One can show that the system matrix of extended transfer function $G(s)s$ remains Hurwitz and the new pair $[\mathbf{A}^*, \mathbf{b}^*]$ is controllable as well. Inspecting the $\delta(\cdot)$-nonlinearity one can see that this belongs to the sector $[0, \infty]$, cf. with (37), so that $1/k_2 \to 0$. Note that here the k_2-value is not necessarily the same as in case of γ-nonlinearity discussed above. Evaluating (38) yields that the Popov plot of $G(s)s$ lies always in the right half-plane, while it $\to 0$ for $\omega \to 0$ and to some negative value on the imaginary axis for $\omega \to \infty$. Since (39), correspondingly (26), constitutes the upper boundary case of h-discontinuity at x reversal, it is apparent that any piecewise continuous hysteresis branches, after the $\dot{x}$-sign changes, will lead to $k_2 < \infty$. Therefore $-1/k_2$ will always lies left-hand-side from the origin of the Popov plot, even if infinitesimally close to zero from the left. For this locus one can always find a strictly positive σ so that the $1/\sigma$ slope is not intersecting the polar plot. This implies that the third condition of the Popov's criterion is also fulfilled. As implication, the $G(s)s\delta$ loop is equally stable. The Popov plot, for the numerical values assigned in Section V.C, is exemplary shown in Fig. 6.

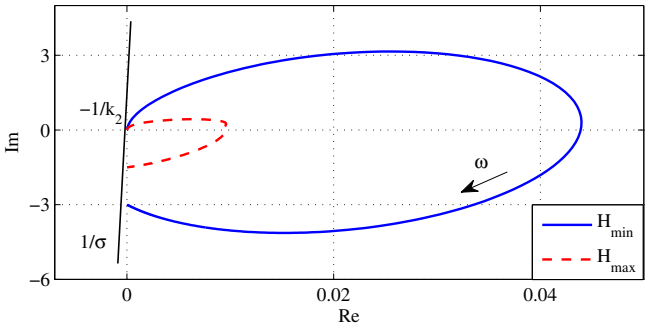

Fig. 6. Popov plots of system $G(s)s$ with feedback nonlinearity $c\,\mathrm{sign}(\dot{y})$.

C. Numerical example

In this Section a numerical example of the closed loop behavior (5), (6) with the VTS-based torsion feedback, i.e. $K_p\tilde{x}$ on the right-hand-side of (6), is shown. Once, the torsion-torque map is assumed according to (34), and once according to (39). The nonlinear static map is assumed as a cubic polynomial function $\gamma(y) = py^3$, and the link inertia is set to its upper bound $H_{\max}$. The VTS is implemented according to Section III while β is assumed to be zero for the sake of simplicity. All parameters used in the numerical setup are listed in Table I. For exciting sufficiently the joint oscillations, the step-wise

TABLE I
PARAMETERS OF NUMERICAL SIMULATION

Param.	Value	Param.	Value	Param.	Value
J	1	D	5	K_p	10.000
$H_{\min}$	0.5	k	10.000	K_d	200
$H_{\max}$	2	p	10.000	L	10
g	2.000	c	1.000	$e(0)$	1

conditions are realized by assuming $0.2x(\infty) \approx e(0) \neq 0$. Note that all parameters are assumed without giving explicit physical units so that the unitless motion states are equally assumed. This allows one for an arbitrary system scaling, while the time argument is conventionally kept in seconds. To allow for a substantial joint torque, and correspondingly torsion, at steady-state conditions the case of a gravity impact is additionally demonstrated. For that the left-hand-side of (5) is modified by adding a positive g-term, which summarizes the gravity constant, mass, and lever arm of the link, and can be assumed as constant for the small displacements e. Recall that non-zero gravity provokes both, transient and steady-state deflections of a flexible joint, and therefore end-position errors of the robot link. The time response of the e and q trajectories are show in Fig. 7. The upper plots (a) and (b)

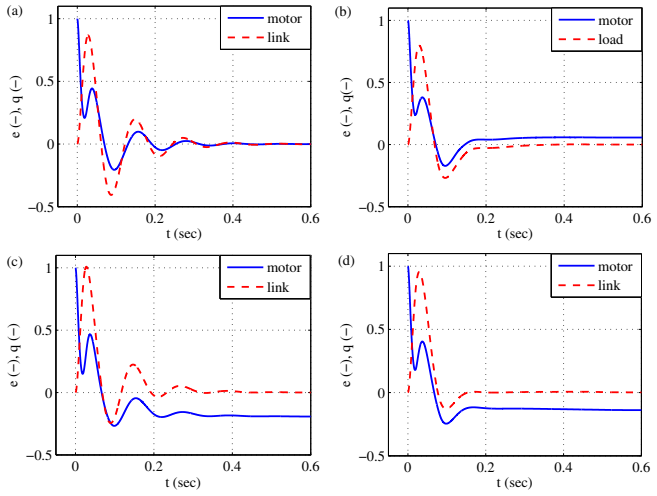

Fig. 7. Motor and link position response: (a) none-hysteresis none-gravity, (b) hysteresis none-gravity, (c) none-hysteresis gravity, (d) hysteresis gravity.

correspond to the case without gravity, and the lower plots (c) and (d) to the case with gravity. The none-hysteresis case (34) is shown in the left-hand-side plots (a) and (c) and the hysteresis case (39) is shown on the right plots in (b) and (d). With the same classification of all four cases the phase portrait in the $(x, \dot{x})$ coordinates are shown in Fig. 8. All four cases disclose a moderate oscillation of the joint torsion which converge to an equilibrium together with the control

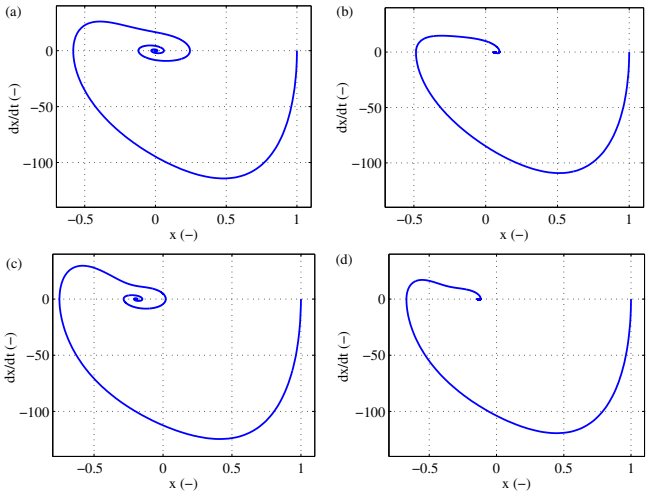

Fig. 8. Joint torsion phase portrait: (a) none-hysteresis none-gravity, (b) hysteresis none-gravity, (c) none-hysteresis gravity, (d) hysteresis gravity.

error. Note that in both cases of gravity and hysteresis, it is the link position and not the motor one which reaches zero steady-state, therefore confirming the purpose of the VTS to compensate for the joint torsion errors. Recall that the primary goal of VTS is in improving the link position accuracy, while the motor position can deviate from zero steady-state, therefore explicitly accounting for the relative joint torsion.

VI. CONCLUSIONS

In this paper the absolute stability of including the virtual torsion sensor (VTS) in the position control loop of flexible robotic joints have been shown. The analysis started by exposing the dissipativity and sector-conditioned passivity of the torsion-torque hysteresis map. Considering two boundary cases of zero and maximal energy dissipation per reversal cycle, the absolute stability in the Popov sense has been proved after appropriate loop transformations. Numerical examples visualize the results of analysis and provide some practical hints for the use of VTS in the underlying robot joint position control.

REFERENCES

[1] M. W. Spong, "Modeling and control of elastic joint robots," *Journal of Dynamic Systems, Measurement, and Control*, vol. 109, no. 4, pp. 310–319, 1987.
[2] J. Hung, "Control of industrial robots that have transmission elasticity," *IEEE Trans. on Industrial Electronics*, vol. 38, no. 6, pp. 421–427, 1991.
[3] M. Jankovic, "Observer based control for elastic joint robots," *IEEE Trans. on Robotics and Automation*, vol. 11, no. 4, pp. 618–623, 1995.
[4] R. Ortega, R. Kelly, and A. Loría, "A class of output feedback globally stabilizing controllers for flexible joints robots," *IEEE Trans. on Robotics and Automation*, vol. 11, no. 5, pp. 766–770, 1995.
[5] W.-H. Zhu, E. Dupuis, M. Doyon, and J.-C. Piedboeuf, "Adaptive control of harmonic drives based on virtual decomposition," *IEEE/ASME Transactions on Mechatronics*, vol. 11, no. 5, pp. 604–614, 2006.
[6] A. Albu-Schaeffer, C. Ott, and G. Hirzinger, "A unified passivity based control framework for position, torque and impedance control of flexible joint robots," in *Robotics Research*, ser. Springer Tracts in Advanced Robotics. Springer, 2007, vol. 28, pp. 5–21.
[7] A. De Luca, D. Schroder, and M. Thummel, "An acceleration-based state observer for robot manipulators with elastic joints," in *IEEE Int. Conference on Robotics and Automation*, 2007, pp. 3817–3823.
[8] P. Axelsson, R. Karlsson, and M. Norrlöf, "Bayesian state estimation of a flexible industrial robot," *Control Engineering Practice*, vol. 20, no. 11, pp. 1220–1228, 2012.
[9] N. Mansfeld and S. Haddadin, "A comparison of braking strategies for elastic joint robots," in *IEEE Int. Conference on Robotics and Automation*, 2015, pp. 789–796.
[10] M. Ruderman, F. Hoffmann, and T. Bertram, "Modeling and identification of elastic robot joints with hysteresis and backlash," *IEEE Trans. on Industrial Electronics*, vol. 56, no. 10, pp. 3840–3847, 2009.
[11] F. Ghorbel, J. Hung, and M. Spong, "Adaptive control of flexible-joint manipulators," *IEEE Cont. Syst. Mag.*, vol. 9, no. 7, pp. 9–13, dec. 1989.
[12] P. Tomei, "A simple PD controller for robots with elastic joints," *IEEE Trans. on Automatic Control*, vol. 36, no. 10, pp. 1208–1213, 1991.
[13] R. Kelly and V. Santibánez, "Global regulation of elastic joint robots based on energy shaping," *IEEE Trans. on Automatic Control*, vol. 43, no. 10, pp. 1451–1456, 1998.
[14] A. De Luca and P. Lucibello, "A general algorithm for dynamic feedback linearization of robots with elastic joints," in *IEEE Int. Conference on Robotics and Automation (ICRA)*, 1998, pp. 504–510.
[15] A. De Luca, "Feedforward/feedback laws for the control of flexible robots," in *IEEE International Conference on Robotics and Automation (ICRA)*, vol. 1, 2000, pp. 233–240.
[16] N. Kircanski, A. Goldenberg, and S. Jia, "An experimental study of nonlinear stiffness, hysteresis, and friction effects in robot joints with harmonic drives and torque sensors," in *Experimental Robotics III*. Springer, 1994, vol. 200, pp. 326–340.
[17] W. Seyfferth, A. J. Maghzal, and J. Angeles, "Nonlinear modeling and parameter identification of harmonic drive robotic transmissions," in *Proc. IEEE International Conference on Robotics and Automation (ICRA'95)*, vol. 3, 1995, pp. 3027–3032.
[18] H. D. Taghirad and P. R. Bélanger, "Modeling and parameter identification of harmonic drive systems," *Journal of Dynamic Systems, Measurement, and Control*, vol. 120, no. 4, pp. 439–444, 1998.
[19] R. Dhaouadi, F. H. Ghorbel, and P. S. Gandhi, "A new dynamic model of hysteresis in harmonic drives," *IEEE Trans. on Industrial Electronics*, vol. 50, no. 6, pp. 1165–1171, 2003.
[20] T. Tjahjowidodo, F. Al-Bender, and H. V. Brussel, "Nonlinear modelling and identification of torsional behaviour in Harmonic Drives," in *Proc. International Conference on Noise and Vibration Engineering (ISMA2006)*, 2006, pp. 2785–2796.
[21] R. Bischoff, J. Kurth, G. Schreiber, R. Koeppe, A. Albu-Schaeffer, A. Beyer, O. Eiberger, S. Haddadin, A. Stemmer, G. Grunwald, and G. Hirzinger, "The KUKA-DLR lightweight robot arm - a new reference platform for robotics research and manufacturing," in *41st International Symposium on Robotics (ISR) and 6th German Conference on Robotics (ROBOTIK)*, 2010, pp. 1–8.
[22] S. Wolf, G. Grioli, O. Eiberger, W. Friedl, M. Grebenstein, H. Höppner, E. Burdet, D. G. Caldwell, R. Carloni, M. G. Catalano *et al.*, "Variable stiffness actuators: Review on design and components," *IEEE/ASME transactions on mechatronics*, vol. 21, no. 5, pp. 2418–2430, 2016.
[23] D. J. Hill and P. J. Moylan, "Stability results for nonlinear feedback systems," *Automatica*, vol. 13, no. 4, pp. 377–382, 1977.
[24] C. I. Byrnes, A. Isidori, and J. C. Willems, "Passivity, feedback equivalence, and the global stabilization of minimum phase nonlinear systems," *IEEE Transactions on automatic control*, vol. 36, no. 11, pp. 1228–1240, 1991.
[25] H. K. Khalil, *Noninear Systems*, 3rd ed. Pearson, 2001.
[26] N. E. Barabanov and V. A. Yakubovich, "Absolute stability of control systems having one hysteresis-like nonlinearity," *Avtomatika i Telemekhanika*, no. 12, pp. 5–12, 1979.
[27] A. Hassibi, S. P. Boyd, and J. P. How, "A class of lyapunov functionals for analyzing hybrid dynamical systems," in *American Control Conference (ACC'99)*, 1999, pp. 2455–2460.
[28] R. B. Gorbet, K. A. Morris, and D. W. Wang, "Passivity-based stability and control of hysteresis in smart actuators," *IEEE Transactions on control systems technology*, vol. 9, no. 1, pp. 5–16, 2001.
[29] R. Ouyang and B. Jayawardhana, "Absolute stability analysis of linear systems with duhem hysteresis operator," *Automatica*, vol. 50, no. 7, pp. 1860–1866, 2014.
[30] J. Oh and D. S. Bernstein, "Semilinear duhem model for rate-independent and rate-dependent hysteresis," *IEEE Transactions on Automatic Control*, vol. 50, no. 5, pp. 631–645, 2005.
[31] M. Ruderman, T. Bertram, and M. Iwasaki, "Modeling, observation, and control of hysteresis torsion in elastic robot joints," *Mechatronics*, vol. 24, no. 5, pp. 407–415, 2014.

[32] M. Ruderman and M. Iwasaki, "On identification and sensorless control of nonlinear torsion in elastic robotic joints," in *IEEE 40th Anual Conference Industrial Electronics Society*, 2014, pp. 2828–2833.
[33] M. Ruderman and M. Iwasaki, "Sensorless torsion control of elastic joint robots with hysteresis and friction," *IEEE Transactions on Industrial Electronics*, vol. PP, no. 99, pp. 1–1, 2015.
[34] M. Ruderman, "Compensation of nonlinear torsion in flexible joint robots: Comparison of two approaches," *IEEE Transactions on Industrial Electronics*, vol. 63, no. 9, pp. 5744–5751, 2016.
[35] M. Ruderman, "On stability and robustness of virtual torsion sensor (VTS) for flexible joint robots," in *IEEE 42nd Annual Conference of the Industrial Electronics Society*, 2016, pp. 6984–6899.
[36] M. W. Spong, S. Hutchinson, and M. Vidyasagar, *Robot modeling and control*. Wiley, 2006.
[37] B. Siciliano, L. Sciavicco, L. Villani, and G. Oriolo, *Robotics: modelling, planning and control*. Springer, 2009.
[38] M. Ruderman and M. Iwasaki, "On damping characteristics of frictional hysteresis in pre-sliding range," in *Journal of Physics: Conference Series*, vol. 727, no. 1, 2016, p. 012014.
[39] M. Ruderman and D. Rachinskii, "Use of prandtl-ishlinskii hysteresis operators for coulomb friction modeling with presliding," in *Journal of Physics: Conference Series*, vol. 811, no. 1, 2017, p. 012013.
[40] A. De Luca, "Feedforward/feedback laws for the control of flexible robots," in *IEEE International Conference on Robotics and Automation (ICRA'00)*, 2000, pp. 233–240.
[41] C. De Persis and A. Isidori, "A geometric approach to nonlinear fault detection and isolation," *IEEE Trans. on Automatic Control*, vol. 46, no. 6, pp. 853–865, 2001.
[42] A. De Luca and R. Mattone, "Actuator failure detection and isolation using generalized momenta," in *Proc. IEEE International Conference on Robotics and Automation (ICRA'03)*, 2003, pp. 634–639.
[43] J. Chaboche, "A review of some plasticity and viscoplasticity constitutive theories," *Int. J. of Plasticity*, vol. 24, no. 10, pp. 1642–1693, 2008.
[44] M. Ruderman and M. Iwasaki, "Impact of hysteresis lost motion on the sensorless torsion control of elastic robotic joints," in *IEEE International Conference on Mechatronics (ICM2015)*, 2015, pp. 650–655.
[45] R. Ortega, J. A. L. Perez, P. J. Nicklasson, and H. Sira-Ramirez, *Passivity-based control of Euler-Lagrange systems: mechanical, electrical and electromechanical applications*, 1st ed. Springer, 1998.
[46] J. C. Willems, "Dissipative dynamical systems part I: General theory," *Archive for rational mech. and anal.*, vol. 45, no. 5, pp. 321–351, 1972.
[47] G. Zames, "On the input-output stability of time-varying nonlinear feedback systems part one: Conditions derived using concepts of loop gain, conicity, and positivity," *IEEE transactions on automatic control*, vol. 11, no. 2, pp. 228–238, 1966.
[48] J.-J. Slotine and W. Li, *Applied Nonlinear Control*. Prentice Hall, 1991.